EurJIC
European Journal of Inorganic Chemistry

Minireview
doi.org/10.1002/ejic.201901291

Chemistry Europe
European Chemical Societies Publishing

Phosphonate MOFs

Probing Isoreticular Expansions in Phosphonate MOFs and their Applications

Patrik Tholen,[a] Yunus Zorlu,[b] Jens Beckmann,*[c] and Gündoğ Yücesan,*[a]

Abstract: This review is divided into three different parts. In the introduction, the current applications of metal-organic frameworks (MOFs) are shown. Furthermore, the overall stability, a comparison of phosphonate MOFs with carboxylate MOFs, the structural richness of phosphonate MOFs with the challenge in synthesis and different linker geometries is discussed. In the second part, several phosphonate MOFs with Y-shaped planar, X-shaped planar, and X-shaped tetrahedral linker systems are described. The final part discusses different structures of inorganic building units (IBUs) with different metal atoms and a comparison of the formed MOF structures.

Introduction

The systematic synthesis of microporous metal organic frameworks (MOFs) has spawned wide interest in early 2000s for their gas storage properties and sequestration of greenhouse gases.[1,2] As MOF research kept growing, distinct applications in diverse fields, such as catalysis, gas adsorption, drug delivery, food transportation, solar cells, conductivity, proton conductivity, biomimetic chemistry, magnetism etc., have emerged.[3–28] The limitless linker geometries,[29] possibility of attaching reactive organic functional groups around linker scaffolds have created new chemistry namely post synthetic modifications to further optimize the MOF properties.[30–33] To date, the greatest majority of the reported MOFs are synthesized using the phenylcarboxylate derivatives that has trigonal planar metal binding unit fabricating precise metal binding modes.[34,35] Therefore, carboxylate MOFs produced persistent molecular inorganic building units (IBUs) in the shape of paddle wheels or persistent rod shaped IBUs to form the basics or reticular chemistry in this system.[35] Despite the high number of carboxylate MOFs reported in the structure, the industrial applications of MOFs somewhat remained limited due to the presence of carbonyl bonds in the carboxylate metal binding unit, which makes the carboxylate MOFs more prone to hydrolysis.[36] Therefore, one of the growth points of MOF chemistry should be the use of new metal binding units, which could generate chemically and thermally stable MOFs to perform the functions under harsh conditions. The ideal MOF family should also provide extreme structural richness compared to traditional MOFs.

In this sense, phosphonate metal organic frameworks (phosphonate MOFs) form a distinct family of MOFs that exhibit exceptional thermal and chemical stabilities compared to the conventional MOFs.[37–39] Amongst all known MOFs, the phosphonate-based frameworks play only a niche role so far.[38] Despite the limited number of phosphonate MOFs reported in the literature they have already created diverse applications in proton conductivity, catalysis, magnetism etc.,[40–43] and they exhibit potential in forming future non-toxic MOFs, which are suitable for biological and food chemistry applications.[44] The recent interest in phosphonate MOFs have been summarized in several review articles.[37–40,45–47] One of the distinctive natures of phosphonic acid metal binding group is the rich structural diversity observed in this system.[38,48,49] The structural richness of phosphonate metal binding modes could reflect in more diverse applications compared to the traditional MOF families.[38] On the other hand, uncontrolled structural diversity could lead to unexpected growth of inorganic building units of phosphonate MOFs creating random compounds.[49,50] To date, design patterns or strategies in forming predictable porous structures in phosphonate linkers have not been identified yet. In order to create isoreticular expansion or create well-defined pore sizes in this system, such design patterns are needed within the MOF community to create new phosphonate MOFs that could combine near zeolite stabilities with the organic functionalities.

The unique and numeric nomenclature of metal binding modes of phosphonate group have been summarized by Harris and Chandrasekhar.[48,49] The rich metal binding modes of phosphonate MOFs originate from the multiple protonation modes of R-PO_3H_2, the possibilities of coordinate covalent and ionic bonding combinations and rich charge balance efforts to

[a] *Technische Universität Berlin,*
Institute of Food Technology and Food Chemistry, Department of Food Chemistry and Toxicology,
TIB 4/3-3, Gustav-Meyer-Allee 25, 13355 Berlin, Germany
E-mail: yuecesan@tu-berlin.de
[b] *Department of Chemistry, Gebze Technical University, Gebze, 41400 Kocaeli, Turkey*
[c] *Institut für Anorganische Chemie und Kristallographie, Universität Bremen, Leobener Str. 7, 28359 Bremen, Germany*
E-mail: j.beckmann@uni-bremen.de
ORCID(s) from the author(s) for this article is/are available on the WWW under https://doi.org/10.1002/ejic.201901291.

Minireview
doi.org/10.1002/ejic.201901291

compensate the multiple protonation modes of the R-PO_3H_2 metal binding unit. In addition, the strong non-covalent interactions, such as the presence of strong hydrogen bonding between the phosphonate metal binding units, is another structural factor contributing to the structural diversity.[42,51] Traditional lamellar or pillared layered dense phosphonate metal organic solids are constructed with alkyldiphosphonic acid, or linear phenyldiphosphonic acids. Once such phosphonate linkers form metal organic solids, hydrophilic R-PO_3H_2 metal binding units and the hydrophobic linker cores create layered and pillared motifs similar to phospholipid bilayers observed in the cell membranes.[37, 39, 51–55] Therefore, in order to introduce porosity into phosphonate MOFs our group and others have employed two different types of linker geometries to disrupt the dense lamellar and pillared-layered patterns observed in phosphonate MOFs.[56] The first strategy is to use tetrahedral linker cores expanding into three dimensions based one methane and silane cores.[56–59] Such linker geometries prohibited the formation of hydrophobic layers and created the large pore sites. The second approach relied on planar tritopic and tetratopic linkers where the phosphonate arms are separated by 90° and 120° angles.[44,45,60–66] Although, such planar linkers follow the same mechanism of crystallization observed in pillared layered and lamellar phosphonates. The unique geometry of the Y and X shaped linkers generate hexagonal or rectangular void channels with one-dimensional inorganic building units.[38] These recent efforts to synthesize phosphonate MOFs with linkers having Y, X-tetrahedral and X-planar geometries created the first persistent building units in phosphonate-MOF chemistry to achieve isoreticular expansions in this system.

In this minireview, we are summarizing the molecular and one-dimensional IBUs observed in phosphonate MOFs with Y, X-tetrahedral and X-planar geometries to derive persistent inorganic building units to establish the reticular chemistry in this system. We further comment on the conformations of observed IBUs and how the structural evolution of phosphonate MOFs could be achieved. While explaining the structural chemistry of the phosphonate MOFs, we also comment about the applications of the phosphonate MOFs and structural relations in detail in this work.

Y-Shaped Phosphonate Linkers

Linkers with Y-shaped geometry have 120° of separation between the phosphonic acid metal binding groups. Due to the nature of the planar linker, it is not expected to observe lamellar networks with one-dimensional IBUs and three-dimensional pillared-layer networks with two-dimensional sheet-like IBUs. It is more expected, once they form MOFs with one-dimensional IBUs to produce hexagonal void channels. A first example can be seen in the in the following pictures (Figure 1).

Patrik Tholen was born in Aurich/Ostfriesland in Germany in 1989. He finished his B. Sc. and M. Sc. at Carl-von-Ossietzky University in Oldenburg in 2013 and 2018. He is now working in the research group of Dr. G. Yücesan at TU Berlin in the Institute of Food Technology and Food Chemistry toward his Ph. D. His research interests cover the preparation of phosphonate MOFs with X-shaped tetrahedral linker systems and their applications.

Yunus Zorlu carried out his Ph.D. on non-ionic water soluble symmetrical and unsymmetrical phthalocyanine photosensitizers for photodynamic therapy (PDT) of cancer under the supervision of Dr. Fabienne Dumoulin. After a background in inorganic chemistry, he was then appointed research scientist position in the field of structural chemistry in 2008, then associate professor in 2015 in Gebze Technical University. His research interests are mainly focused on development of functional porous materials (metal-organic frameworks (MOFs), non-covalent interactions (halogen and tetrel bondings), crystal engineering of porphyrins, cyclophosphazenes, and phthalocyanines.

Jens Beckmann was born in Arnsberg/Westfalen in Germany in 1970. He studied Chemistry at the at the University of Dortmund, where he received his Diploma (1995) and Ph.D. (1999) under the supervision of Prof. Dr. Klaus Jurkschat. As Fedor Lynen Fellow of the Alexander von Humboldt Foundation, he spent two years at Deakin University in Geelong/Australia in the lab of Prof. Dr. Danis Dakternieks before he was appointed for three years as Lecturer. In 2004, we was appointed Assistant Professor at the Free University Berlin in Germany. In 2010 he moved to his current position as Associate Professor at the University of Bremen. His research interests involve the inorganic and organometallic chemistry of the main group elements and the late transition metals.

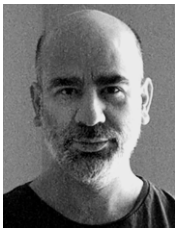

Gündoğ Yücesan was born in Trabzon Turkey in 1976. He finished his B. S. at Boğaziçi University in Istanbul in 2002 and finished his Ph. D. at Syracuse university in NY in 2006. He had his biochemistry postdoc at University of Michigan in Ann Arbor (2006–2008). He worked as an assistant professor at Yıldız Technical University in Istanbul (2011–2016). He is currently working towards his habilitation at TU-Berlin. His research interests include solid state chemistry, semiconductive metal organic frameworks, linker design, fluorescent probes and bioimaging.

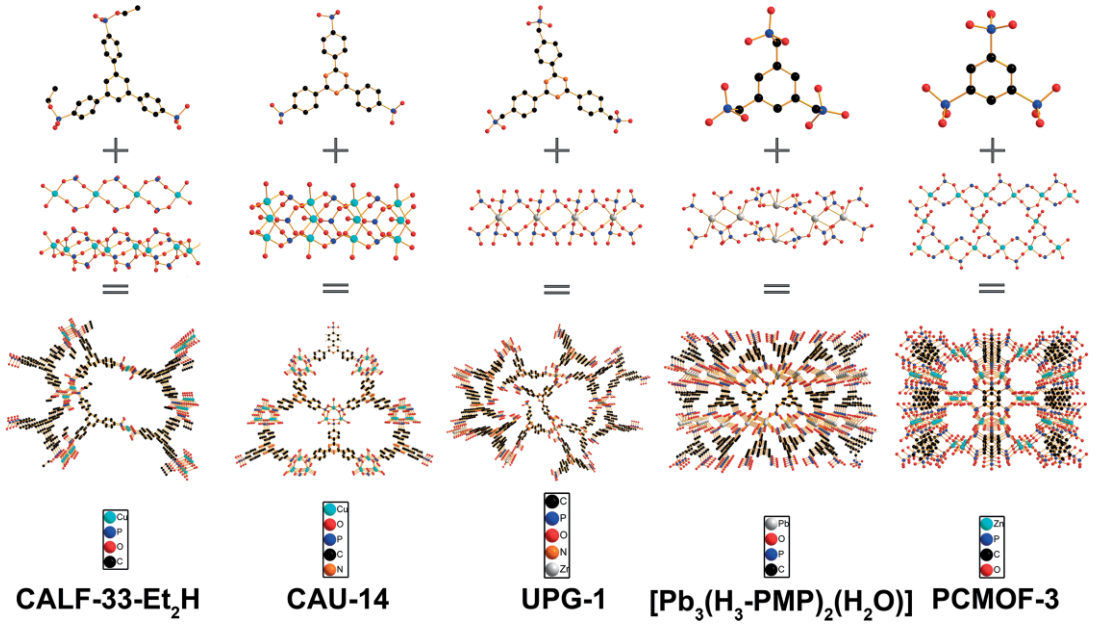

Figure 1. Linker molecule, inorganic building unit and MOF structure of: CALF-33-Et_2H,[61] CAU-14,[66] UPG-1,[70] [$Pb_3(H_3$-PMP)$_2(H_2O)$][71] and PCMOF-3.[72]

CALF-33-Et_2H[61] is based on the linker 1,3,5-*tri*-(phenylene-4-triethoxy phosphane) benzene which was synthesized in three steps according to the literature.[67–69] Suitable crystals for X-ray diffraction were grown from a mixture of $Cu(NO_3)_2$, ligand Et_3H_3-BBP, ethanol, water and 1,3-diisopropylbenzene at 120 °C in a hydrothermal vessel. The blue needle-like crystals were composed of copper-phosphonate pillars which contain two types of copper-phosphonate chains. Square planar copper phosphonate chains and square pyramidal copper-phosphonate mono ethyl ester double chains were connected by stacked Et_2H-BBP^{3-} units to form the three-dimensional framework. One-dimensional pores measuring 7.2 Å × 16.1 Å suitable for N_2 gas sorption were generated. Experimental N_2 gas sorption isotherm gave a calculated Langmuir surface area of 950 $m^2\ g^{-1}$ and a BET surface area of 810 $m^2\ g^{-1}$.

The CALF-33-Et_2H is composed of two distinct one-dimensional inorganic building units (Figure 1). The first one-dimensional IBU is composed of edge touching 8 membered rings of Cu–O–P–O–Cu–O–P–O (further methodically called s.pl.-Cu-8mpr, square planar-Cu-8 membered phosphonate ring) and the second IBU structure is composed of two of IBUs composed of two s.py.-Cu-8mpr, which are connected via copper dimers to the final shape of the second IBU. The second IBU is more complex and the copper centers are square pyramidal due to the presence copper dimers. Therefore, the CALF-33-Et_2H structure has two distinct type of hexagonal and parallelogram void channels.

CAU-14[66] is based on the linker 2,4,6-*tri*-(phenylene-4-phosphonic acid)-*s*-triazine linker (H_6PPT) and was obtained by the reaction of the linker (H_6-PPT) in a mixture of $Cu(NO_3)_2$, NaOH solution and water at 190 °C. The crystal structure shows corner-sharing trimeric $Cu_3O_9(H_2O)_3$ units composed of three distorted square-pyramidal Cu^{2+} ions. The Cu^{2+} ions are coordinated by four different phosphonate groups and an additional water molecule. Each $Cu_3O_9(H_2O)_3$ cluster combines into a one-dimensional chain which is connected to adjacent chains via the linker H_3-TPP^{3-} to form a three-dimensional honey-comb like framework. The generated pores are measuring 9.4 Å in diameter (Figure 1). Interestingly, the crystals are thermal stable up to 380 °C and experimental N_2 gas sorption isotherm gave a calculated BET surface area of 647 $m^2\ g^{-1}$. Also CAU-14 is suitable to reversible take up water without loss of crystallinity.

UPG-1[70] is based on the linker 2,4,6-*tri*-(4-(phosphonomethyl)phenyl)-1,3,5-triazine linker (H_6-TTBMP) and a similar IBU observed in CALF-33-Et_2H. The only difference is that the 1D IBU in CALF-33-Et_2H is composed of tetrahedral copper while UPG-1 is composed of octahedral zirconium within the chain structure (Figure 1). UPG-1 was obtained by the reaction of the linker (H_6-TTBMP) in a mixture of water, methanol, $ZrOCl_2$ and HF as mineralizer at 80 °C. The three-dimensional framework is based on one-dimensional zirconia-phosphonate chains with o-Zr-8mpr connected by H_6-TTBMP ligands. Each ZrO_6 octahedral consists of two monodentate and four bidentate phosphonate tetrahedral from six different phosphonate groups. In addition to the monodentate and bidentate phosphonate groups there are non-coordinating phosphonate groups in the crystal lattice. There are two types of void channels observed in UPG-1, the first one is formed via the hydrogen bonding interactions of the fully protonated phosphonic acid ends lined by free P–O groups and a diameter of about 5 Å. The second void channel is observed as distorted hexagonal void with a diameter of about 10 Å and is composed of four linkers molecules coordinating to the 1D IBU nodes (Figure 1). In comparison with the H_6-PPT ligand (benzene 1,3,5-*tri*-4-phenylphosphonic acid) the H_6-TTBMP is more flexible and the functional groups are out-of-plane with respect to the aromatic ring which allows different connections to the Zr^{4+} ion. Experimental data of CO_2 adsorption at 195 K shows a calculated BET and Langmuir surface area of 410 $m^2\ g^{-1}$ and 514 $m^2\ g^{-1}$. In addition to that the framework shows efficient adsorption of hydrocarbons due to CH – π inter-

actions and a thermal stability up to 430 °C. Overall, the structure of UPG-1 is marvelous with starshaped hydrogen bonded pattern is surrounded by hexagonal void channels observed with Y-shaped linkers. UPG-1 is the clear indication of additional functionalities like hydrogen-bonded networks and hexagonal MOF channels could be together in the same MOF due to the structural diversity of phosphonate MOFs.

Taddei recently continued the work to synthesize UPG-2 with the same Y shaped linker where the methylphosphonate groups are located at meta position. Due to the slightly hindered meta position, the molecular IBU of two-dimensional UPG-2 is composed of the isolated 8 membered rings observed in 1D IBU of UPG-1.[60]

$[Pb_3(H_3\text{-}PMP)_2(H_2O)]$[71] is based on the linker benzene 1,3,5-*tri*-(4-(phosphonomethyl)phenyl) and was obtained by the reaction with $Pb(CH_3COO)_2$. The framework consists of two types of Pb^{2+} ions, two triply deprotonated trisphosphonate ligands $(H_3\text{-}PMP)^{3-}$ and one aqua ligand (Figure 1). The Pb^{2+} ions are coordinated by five oxygen atoms in distorted PO_5 square pyramids and can be differentiated in two groups. Two Pb^{2+} ions are coordinated by four phosphonate oxygen atoms of two different trisphosphonate ligands in basal position and an additional aqua ligand in apical position. The other two Pb^{2+} ions are coordinated by five phosphonate oxygen atoms from five different trisphosphonate ligands and their square pyramids share a common edge and pointing in different directions. This generates s.py.-Pb-16mpr which alternate with $\{Pb_2O_2\}$ units to form one-dimensional chains. Two chains are connected by the $H_3\text{-}PMP^{3-}$ linker to form the three-dimensional framework. The framework got slits with sizes of 4.4 Å × 8.2 Å and 3.5 Å × 8.2 Å and decomposes at temperatures of 245 °C.

PCMOF-3[72] is based on the linker 1,3,5-benzenetriphonsphonic acid and was obtained by diffusion of acetone into a mixture of $Zn(ClO_4)\cdot 6H_2O$, linker and water. The framework consists of two different types Zn^{2+} ions. One is coordinated by four oxygen atoms of four different triphosphonate ligands and forms t-Zn-8mpr which are connecting to one-dimensional chains (Figure 1). The other Zn^{2+} ion is coordinated by two oxygen atoms of two different triphosphonate ligands and two water molecules. The one-dimensional chains are connected by the linker molecules and the second Zn^{2+} ion forming a three-dimensional framework. In addition, the linkers are forming π-stacked dimers with a distance of ⊥d = 3.718(5) Å. Proton conductivity in H_2 at 25 °C and 98 % relative humidity was measured with 3.5 × 10–5 S cm^{-1} and 4.5 × 10–8 S cm^{-1} at 25 °C and 44 % relative humidity. The well-ordered chains of aqua ligands serve as main source of protons. With an activations energy for proton transfer with E = 0.17 eV, the Grotthuss proton transfer mechanism was proven.

The two-dimensional IBU of PCMOF-3 is composed of the classical one-dimensional IBU with edge touching 8 membered M–O–P–O–M–O–P–O rings, which are connected by the second Zn^{2+} ion to give the final structure of the two-dimensional building units. The short length of the Y-shaped linker in this study was influential for the oligomerization of inorganic components into two dimensions, while longer tether lengths prove longer distances between the one-dimensional IBUs and there is not enough space for the second zinc ion to connect the one-dimensional chains.

Planar X-shaped organophosphonic acid linker 5,10,15,20-Tetrakis(*p*-phenylphosphonic acid) porphyrin (H_8TPPA)

H_8-TPPA is an interesting linker where the four phosphonic acid metal binding units are separated by 90° of angle. Therefore, it is expected that once H_8-TPPA is connected to four linear IBUs, it would produce a MOF structure with rectangular void channels. It is related to the tetrakis(*p*-carboxyphenyl) porphyrin which porphyrin MOFs are also used for catalytic applications.[73–76] Even a heme-like biomimetic system with ultra-large pore size, high water stability and catalytically active centers[77] and thermally high stable Zr-MOFs[78] are possible. Also the most recent review article on stable MOFs should be mentioned at this point[79] This could lead to an interesting field for the more stable phosphonate porphyrin MOFs. Due to the unique nature of the planar linker, it is not expected to observe lamellar networks unless H_8-TPPA has two fully protonated phosphonic acids in the final framework structure. In addition, H_8-TPPA can provide up to 10 negative charges with the deprotonation of hydrogen in the porphyrin ring. Therefore, H_8-TPPA is a very suitable linker to form MOFs with trivalent and tetravalent metals in addition to the divalent metals commonly used in MOF synthesis.

Co-CAU-36[80] is based on the linker nickel 5,10,15,20-tetrakis(*p*-phenylphosphonic acid) porphyrin and was obtained by reaction with a mixture of linker, $CoCl_2\cdot 6H_2O$, DABCO, water and HCl solution at 160 °C in a sealed Teflon insert (Figure 2). The Crystal structure was determined of small sized crystals of less than 1 µm using cRED data at low temperature (96 K). The Co atoms are coordinated by four oxygen atoms of four different bidentate phosphonate groups. Within the IBU there are t-Co-8mpr forming a one-dimensional chain. The chains are connected by the porphyrin linkers Ni-H_4- $TPPA^{4-}$ forming a three-dimensional framework. Within this framework pores with a diameter of about 9 Å when occupied by DABCO and about 12.5 Å when empty were generated. Thermal stability up to 350 °C was observed without loss of crystallinity. The BET surface area after gas adsorption with N_2 is 700 $m^2\ g^{-1}$.

Zr-CAU-30[65] is based on the linker nickel 5,10,15,20-tetrakis(*p*-phenylphosphonic acid) porphyrin and was obtained by reaction of a mixture of linker, Zr^{4+} salt, NaF and NaOH solution in a sealed Teflon inlet at 180 °C. The crystal structure consists of corner sharing ZrO_6 octahedral forming a one-dimensional chain with o-Zr-8mpr. Adjacent chains are connected by partly deprotonated Ni-H_2-$TPPA^{6-}$ linker forming a three-dimensional framework. Within this framework pores with the size of 13 Å (edge to edge) or 20 Å (diagonal) were generated. Sorption measurements using N_2 at 77 K were performed and a BET surface area of 970 $m^2\ g^{-1}$ was calculated. The compound is chemical stable in a pH range of pH = 0 – 12 in HCl/NaOH and organic solvents like pure acetic acid, MeOH, EtOH, acetone, DMF and DCM. Surprisingly the crystals are also stable in a 0.1 M phosphate buffer at pH = 7.2. Additionally, thermal stabil-

Minireview
doi.org/10.1002/ejic.201901291

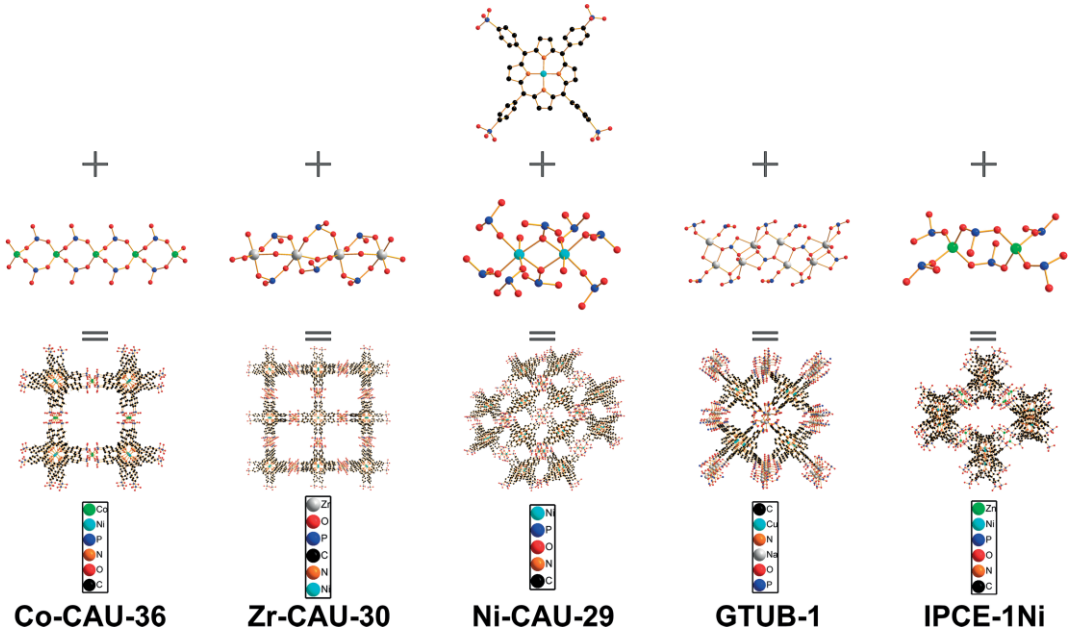

Figure 2. Linker molecule, inorganic building unit and MOF structure of: Co-CAU-36,[80] Zr-CAU-30,[65] Ni-CAU-29,[63] GTUB-1[43] and IPCE-1.[81]

ity was achieved up to 400 °C in air. Cyclic voltammograms of Zr-CAU-30 showed a reversible redox process at a half-wave potential of $E_{1/2}$ = -0.649 V. Cyclic stability was shown by measuring 50 cycles with a scan rate of 250 mV s^{-1}.

Ni-CAU-29[63] is based on the linker nickel 5,10,15,20-tetrakis(*p*-phenylphosphonic acid) porphyrin and it was obtained by reaction of the linker and $NiCl_2$•$6H_2O$ in water at 180 °C (Figure 2). The crystal structure consists of edge-sharing NiO_6 polyhedral forming a Ni_2O_{10} cluster. Eight Ni_2O_{10} units are connected by four different Ni-H_6-$TPPA^{2-}$ linkers forming the three-dimensional framework with one-dimensional pores with sizes of 2.8 Å × 5.0 Å and 3.8 Å × 3.8 Å. During the reaction at 180 °C and 48 h no cleavage of the central Ni^{2+} was observed. The sorption properties were obtained by employing N_2 and H_2O at 77 K and 298 K, respectively. At 77 K no uptake of N_2 was observed probably due to low kinetics. The H_2O uptake was the highest in a series of Ni-, Mn-, Co- and Cd-CAU-29 with 181 mg g^{-1}, 140 mg g^{-1}, 166 mg g^{-1} and 116 mg g^{-1} respectively. Thermal stability was measured by TG up to the collapse of the framework at temperatures higher than 350 °C. Chemical stability was proven by stirring Co-CAU-29 in different solvents for 24 h. Tolerated were aqueous solutions of HCl/NaOH in a pH range of 1 – 11, the organic solvents DCM, EtOH, DMF, acetone, pure acetic acid. At pH of 0 a loss of crystallinity and above pH 11 as well as in phosphate buffer complete decomposition is observed. The proton conductivity at different temperatures and relative humidities and the Arrhenius activation energies E_A were measured by electrochemical impedance spectroscopy and are given in Table 1. Due to the data the Grotthuss mechanism is the prominent pathway for proton conductivity.

GTUB-1[43] is based on the linker copper 5,10,15,20-tetrakis(*p*-phenylphosphonic acid) porphyrin and was obtained by reaction of the linker with $Cu(NO_3)_2$•$3H_2O$, DMF and MeOH at 120 °C (Figure 2). The crystal structure contains edge-sharing

Table 1. Proton conductivity and Arrhenius activation energies E_A at different temperatures and relative humidities.

Relative humidity [%rh]		50	75	90
Conductivity [S cm^{-1}]	80 °C	2.41×10^{-7}	1.35×10^{-6}	5.62×10^{-6}
	100 °C	3.46×10^{-7}	1.78×10^{-6}	5.80×10^{-6}
	120 °C	6.02×10^{-7}	2.60×10^{-6}	6.85×10^{-6}
	140 °C	1.04×10^{-6}	3.42×10^{-6}	7.82×10^{-6}
E_A [eV]		0.34	0.23	0.10

NaO_4 tetrahedrons and NaO_6 polyhedral. Edge-sharing NaO_4 and edge-sharing NaO_6 units with Na-O-Na bridges alternate in one-dimensional chains by O-P-O bridges. The three-dimensional framework consists of connected chains via Cu-H_4-$TPPA^{4-}$ linkers and generates rectangular void channels with dimensions of 9.78 Å × 7.73 Å. In addition, the linkers tend to π-stacking within the three-dimensional framework with a high separation of 3.786 Å and 4.038 Å between the layers. The simulated N_2 adsorption shows a BET surface area of 697 m^2 g^{-1}. Thermal stability was observed up to 400 °C without decomposition. Furthermore, the toxicity on an intestinal cell line, namely Caco-2, was investigated. Cells were treated with different concentrations of GTUB-1 and were analyzed by measuring mitochondrial enzyme activity.[51,82] No cytotoxicity was observed even at higher concentrations.

IPCE-1Ni[81] is based on the linker 5,10,15,20-tetrakis(*p*-phenylphosphonic acid) porphyrin and was obtained by reaction of the linker with a mixture of $Zn(NO_3)_2$•$6H_2O$, phenylphosphonic acid, DMF and H_2O. The crystal framework consists of discrete dinuclear $Zn_2P_6O_{18}$ units forming t-Zn-8mpr (Figure 2). The Zn^{2+} ions are tetragonal coordinated by oxygen atoms of four different Ni-H_3-$TPPA^{5-}$ linker molecules and two bidentate phosphonate groups. Therefore, the linker acts tritopic and is

bonding adjacent inorganic building units to form the tree-dimensional framework. The remaining two phosphonate groups are involved in H-bondings with adjacent linkers. The three-dimensional framework possesses pores of 6.52 Å in diameter which are filled with $CH_3NH_2^+$ ions to compensate the anionic charge. Thermal stability was proven up to 150 °C without change in the framework geometry due to the loss of $(CH_3)NH_2^+$ ions. Between 150 °C and 210 °C a change in the framework geometry and above 300 °C the collapse of the framework is observed. Adsorption of CO_2 at 195 K with activation at 140 °C gave an uptake of 60.9 $cm^3\ g^{-1}$ and calculated BET and Langmuir surface areas of 208.7 $m^2\ g^{-1}$ and 280.3 $m^2\ g^{-1}$. Proton conductivity was proven by impedance spectroscopy at different temperatures and relative humidities with 1.3×10^{-5} S cm^{-1} at 25 °C and 80 % RH as well as 1.55×10^{-3} S cm^{-1} at 75 °C and 80 % RH and an activation energy E_A of 0.86 eV.

CALF-25[83] is based on the linker octaethyl-1,3,6,8-pyrene-tetraphosphonate and was obtained by the reaction of the linker with a mixture of $BaBr_2{\cdot}2H_2O$, EtOH and water through partially hydrolysis in situ at 120 °C. This is the only MOF synthesized using this type of planar tetratopic phosphonate linker in the literature (Figure 3). The crystal structure consists of edge-sharing barium phosphonate polyhedral forming one-dimensional chains which are cross-linked to four additional chains by the pyrene linkers giving a three-dimensional porous framework. Every barium atom is coordinated and saturated by phosphonate monoethyl ester oxygen atoms. The one-dimensional pores are shaped rectangular with site lengths of 4.59 Å × 3.89 Å and are lined with phosphonate ethyl ester groups in the corners as well as the aromatic system of the pyrene core on their walls. Due to a barium atom to linker ratio of 1:1 the three-dimensional framework is acidic. Adsorption of N_2 at 77 K after activation at 100 °C and a pressure of 10^{-5} Torr gave a calculated BET surface area of 385 $m^2\ g^{-1}$. For characterization of the pore surface area properties CO_2 and CH_4 adsorption were performed. Despite the acidic nature of CALF-25 the zero-loading heats of adsorption were found to be 23.9 kJ mol^{-1} for CO_2 and 14.6 kJ mol^{-1} for CH_4. To prove the hydrophobic and weakly polarizing character water vapor sorption was performed. With a calculated heat of adsorption of around 45 kJ mol^{-1} it is comparable to graphite and other hydrophobic MOFs.[84–87] Therefore it suggests that the acidic barium phosphonate chains are shielded by the ethyl ester groups.

Tetrahedral X-shaped organophosphonic acid linkers with methane, silane and adamantane cores

Tetrahedral geometry opens up into three dimensions with ca. 108° of angle where the core is composed of methane, silane and adamantane cores. The first MOF with adamantane core was reported in 2000s by Shimizu and our group reported the first MOF with the methane core in 2015. [38, 40] The unique tetrahedral three-dimensional structure prohibits the formation of highly dense hydrophobic hydrocarbons to form lamellar or pillared layered structures observed in traditional phosphonate metal organic solids.

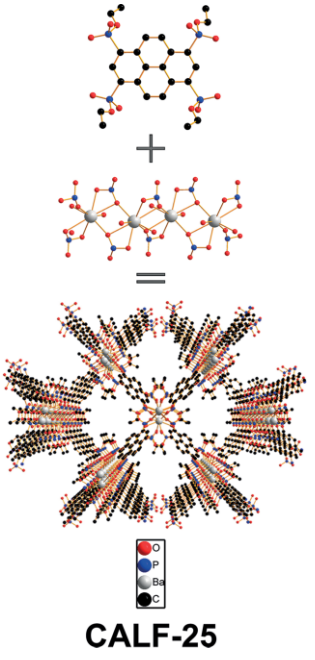

Figure 3. Linker molecule, inorganic building unit and MOF structure of: CALF-25.[83]

$[\{Cu(terpy)\}_4Cu(VO_2)_4(MTPPA\text{-}H)_2]$[88] is based on the linker methane tetra-*p*-phenylphosphonic acid and was obtained by reaction of the linker with a mixture of $CuSO_4{\cdot}5H_2O$, Na_3VO_4, 2,2′:6′:2″-terpyridine, HF and water at 180 °C (Figure 4). The obtained three-dimensional framework consists of a one-dimensional chain containing octahedral coordinated Cu(II) atoms, square-pyramidal coordinated Cu(II) atoms and tetrahedral coordinated V(V) atoms. The octahedral coordinated Cu(II) atom is surrounded by four phosphonate and two VO_4 tetrahedrons. The square-pyramidal coordinated Cu(II) atom is surrounded by two phosphonate tetrahedrons and three nitrogen atoms of the tridentate terpy ligand. The V(V) atoms are surrounded by two phosphonate tetrahedrons, one Cu(II) octahedron and an aqua ligand. While the square pyramidal $[\{Cu(terpy)\}]^{2+}$ units are exclusively coordinated by MTPPA oxygen atoms and act like dead-end clamps, the connection in the three-dimensional framework is due to the tetrahedral V(V) and the octahedral Cu(II) sites. Adjacent one-dimensional chains are connected by MTPPA ligands coordinating to the V(V) sites. For the purpose of this study, the $[\{Cu(terpy)\}]^{2+}$ units should be used as mold-cast templates which can be removed due to decomposition at around 250 °C. In a TGA measurement the sample was heated to 375 °C with 5 °C min^{-1} and kept at this temperature for 75 minutes. A weight loss of 8.6 % due to the loss of water and half of the terpyridine molecules was observed. For final results further investigations are currently done.

$[Co_2H_4\text{-}MTPPA]{\cdot}3\ NMP{\cdot}H_2O$[56] is based on the linker methane tetra-*p*-phenylphosphonic acid and was obtained by the reaction of the linker with $CoSO_4{\cdot}7H_2O$ in NMP at 165 °C (Figure 4). A one-dimensional chain containing t-Co-8mpr is formed. The Co(II) atoms are tetrahedral coordinated by four $R\text{-}PO_3H^{1-}$ units derived from H_4-MTPPA^{4-} linkers. The three-dimensional framework is build up by connecting the chains via

Minireview
doi.org/10.1002/ejic.201901291

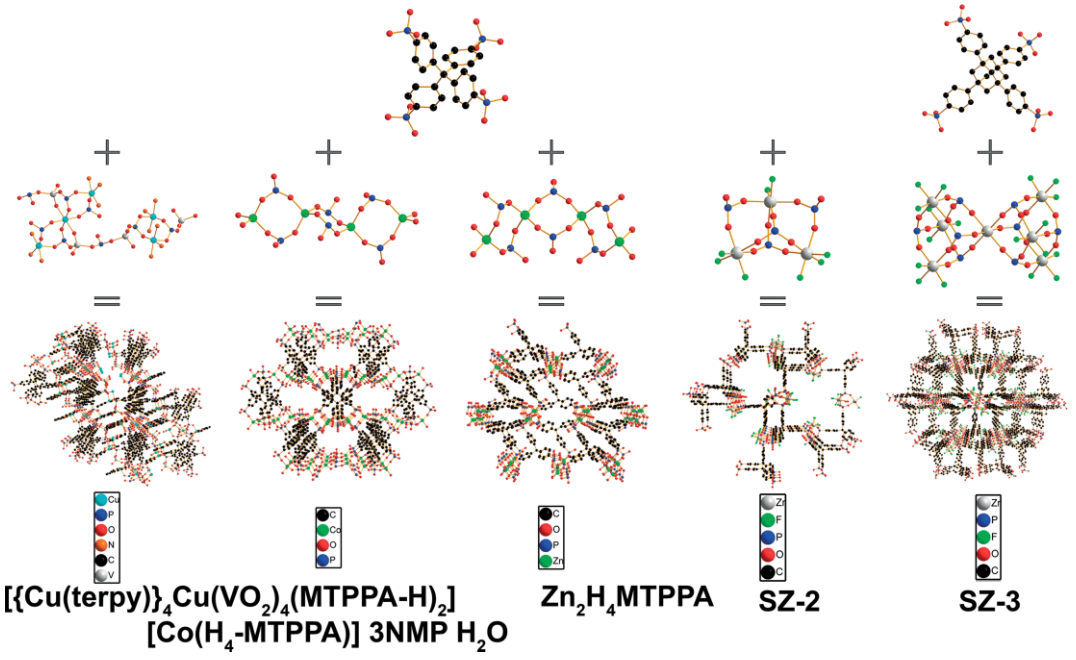

Figure 4. Linker molecule, inorganic building unit and MOF structure of: $[\{Cu(terpy)\}_4Cu(VO_2)_4(MTPPA\text{-}H)_2]$,[88] $[Co(H_4\text{-}MTPPA)]$ 3NMP H_2O,[56] Zn_2H_4MTPPA,[89] SZ-2[59] and SZ-3.[59]

the H_4-MTPPA^{4-} linkers. The calculated BET surface area by simulated N_2 adsorption at 77 K shows 1034 $m^2\,g^{-1}$. Thermal stability was measured by TGA with decomposition at around 525 °C.

Zn_2H_4-MTPPA[56] is based on the linker methane tetra-*p*-phenylphosphonic acid and was obtained by the reaction of the linker with $ZnSO_4{\cdot}7H_2O$ in DMF at 180 °C (Figure 4). A one-dimensional chain containing edge-sharing t-Zn-8mpr is formed. The Zn(II) atoms are tetrahedrally coordinated to four R-PO_3H^{1-} units derived from H_4-MTPPA^{4-} linkers. The three-dimensional framework is build up by connecting the chains via the H_4-MTPPA^{4-} molecules. The calculated BET surface area by simulated N_2 adsorption at 77 K shows 927 $m^2\,g^{-1}$. The void volume was computed with 51.3 % with a 0 Å sized probe and the accessible pore volume was computed with 46.0 % with a helium probe.

SZ-2[59] is based on the linker methane tetra-*p*-phenylphosphonic acid and was obtained by slow diffusion and ionothermal reaction of separated $ZrCl_4$ and H_8-MTPPA into an ionic liquid containing *N*-butyl-*N*-methylpyrrolidinium bromide ([C_4mpyr][Br]) and *N*-ethylpyridinium bromide ([C_2py][Br]) in the presence of HF. ZrO_3F_3 and ZrO_4F_2 moieties are found which are coordinated by three and four MTPPA ligands. Two ZrO_3F_3 and one ZrO_4F_2 units are connected by four bridging CPO_3 groups forming a $Zr_3P_4O_{10}F_8$ cluster (Figure 4). One MTPPA ligand connects four $Zr_3P_4O_{10}F_8$ cluster to form a three-dimensional framework. Adsorption of N_2 resulted in a calculated BET surface area of 225 $m^2\,g^{-1}$ and Langmuir surface area of 375 $m^2\,g^{-1}$. The thermal stability up to 300 °C was found by thermogravimetric analyses. The compound is chemical stable against boiling water and aqueous solutions in a pH range of 1–11.

SZ-3[59] is based on the linker 1,3,5,7(*p*-phenylphosphonic acid) adamantine and was obtained by ionothermal reaction of $ZrCl_4$ and H_8-PPA in an ionic liquid containing *N*-butyl-*N*-methylpyrrolidinium bromide ([C_4mpyr][Br]) and *N*-ethylpyridinium bromide ([C_2py][Br]) in the presence of HF. The ZrO_6 and ZrO_3F_3 moieties are found which are coordinated by six and three bridging PPA ligands. Six ZrO_3F_3 units are connected to one ZrO_6 unit by six corner-sharing phosphonate groups generating a $Zr_7P_8O_{22}F_{16}$ cluster (Figure 4). These $Zr_7P_8O_{22}F_{16}$ clusters are connected by PPA linkers to form the three-dimensional framework. Adsorption of N_2 resulted in a calculated BET surface area of 572 $m^2\,g^{-1}$ and Langmuir surface area of 695 $m^2\,g^{-1}$. The thermal stability up to 210 °C was found by thermogravimetric analyses. The compound is chemical stable against boiling water, aqueous solutions in a pH range of 1–11 and fumic acids including aqua regia, conc. HCl and conc. HNO_3. When SZ-3 is soaked in aqua regia the adsorption of N2 resulted in slightly higher BET and Langmuir surface areas of 594 $m^2\,g^{-1}$ and 732 $m^2\,g^{-1}$.

Tetrahedral X-shaped organophosphonic acid linkers with silane core

Zr-H_4-STPPA[41] is based on the linker tetraphenylsilane tetrakis-4-phosphonic acid, H_8-STPPA, and was obtained by the reaction of the linker with a mixture of $ZrOCl_2{\cdot}8H_2O$, water, methanol and HF at 180 °C. The framework consists of adjacent ZrO_6 octahedrons each connected by four R-PO_3H^{1-} tetrahedrons from the H_4-STPPA linkers (Figure 5). In addition, two monodentate R-PO_3H^{1-} tetrahedrons are connecting adjacent chains to form the three-dimensional framework. Within the chains o-Zr-8mpr were found. The crystals are chemical stable in organic solvents like DMA, *n*-hexane, acetonitrile, 2-propanol, DCM, DMF, methanol, chloroform, ethanol, tetrachloromethane, acetone and propanol as well as in aqueous solutions in a pH

range of 1 – 12, boiling water, conc. HCl, aqua regia and conc. HNO_3. Due to Lewis acid and Brønsted acid sites in the framework heterogeneous catalyzation was tested using styrene oxide and CO_2 in a cycloaddition reaction. Under optimal reaction conditions yields of 95 %, a TON of 2850 with a TOF of 238 h^{-1} were obtained.

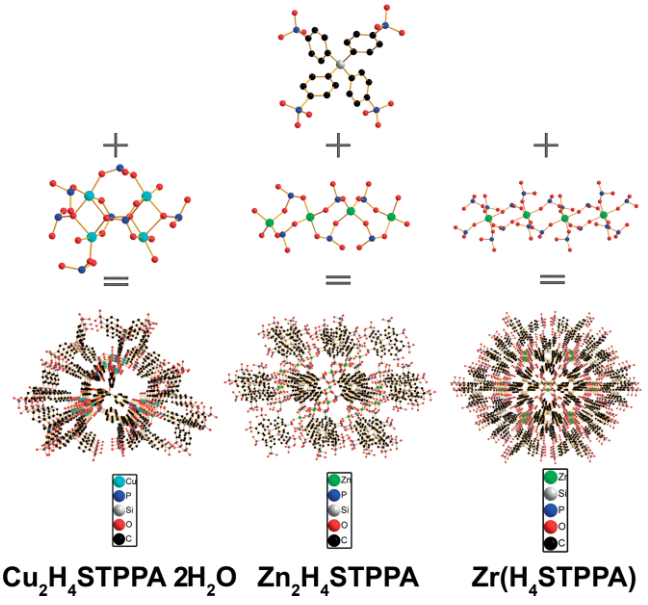

Figure 5. Linker molecule, inorganic building unit and MOF structure of: $Cu_2H_4STPPA\ 2H_2O$,[56] Zn_2H_4STPPA[56] and $Zr(H_4STPPA)$.[41]

Zn_2-H_4-STPPA[56] is based on the linker tetraphenylsilane tetrakis-4-phosphonic acid and was obtained by the reaction of the linker with a mixture of $ZnNO_3$, water and methanol at 150 °C (Figure 5). The framework consists of adjacent ZnO_4 tetrahedrons each connected by four R-PO_3H^{1-} tetrahedrons from the H_4-STPPA linkers forming one-dimensional chains with t-Zn-8mpr. The three-dimensional framework is build up by connecting the chains via the STPPA molecules. The calculated BET surface area by simulated N_2 adsorption at 77 K shows 565 $m^2\ g^{-1}$. The void volume was computed with 48.1 % with a 0 Å sized probe and the accessible pore volume was computed with 33.8 % with a helium probe.

Cu_2-H_4-STPPA·2 H_2O[56] is based on the linker tetraphenylsilane tetrakis-4-phosphonic acid and was obtained by the reaction of the linker with a mixture of $Cu(NO_3)_2$·$3H_2O$, NaOH, water and methanol at 150 °C. The framework shows three distinct phosphonate protonation modes (Figure 5). Reduced to one inorganic building unit it shows one full deprotonated RPO_3^{2-}, one half protonated R-PO_3H^{1-} and two full protonated R-PO_3H_2 groups. The phosphonates coordinate to one square pyramidal Cu^{2+}, two square pyramidal monohydrated $\{Cu(H_2O)\}^{2+}$ and one square pyramidal double hydrated $\{Cu(H_2O)_2\}^{2+}$ forming a $Cu_4P_7O_{25}$ cluster. The $Cu_4P_7O_{25}$ cluster contains two $\{Cu_2O_2\}$ rhombi with alternating short-long Cu-O distances. Adjacent Cu_4 cluster are connected with two STPPA moieties forming the three-dimensional framework. The calculated BET surface area by simulated N_2 adsorption at 77 K shows 794 $m^2\ g^{-1}$. The void volume was computed with 48.7 % with a 0 Å sized probe and the accessible pore volume was computed with 40.0 % with a helium probe.

Structural Comparison of Inorganic Building Units (IBUs)

Tetrahedral Metal Coordination

The common structure in the compounds Co-H_4-MTPPA, Zn_2-H_4-MTPPA, and Zn_2-H_4-STPPA (Figure 6) is the t-M-8mpr (M = metal) with tetrahedral MO_4 and R-PO_3H^{-1} units. These share common edges and can differ in their angles forming a one-dimensional chain. In comparison with the same type of linker (tetra branched MTPPA or STPPA) the BET surface area decreases (Co-H_4-MTPPA: 1034 $m^2\ g^{-1}$, Zn_2-H_4-MTPPA: 927 $m^2\ g^{-1}$, Zn_2-H_4-STPPA: 565 $m^2\ g^{-1}$) with a less straightened chain (156° > 142° > 125°) due to less distance between the linker molecules forming the connection (Figure 7). Therefore, a promising way to maximize the void volume is to generate straight one-dimensional chains to maximize the distance between the organic linkers.

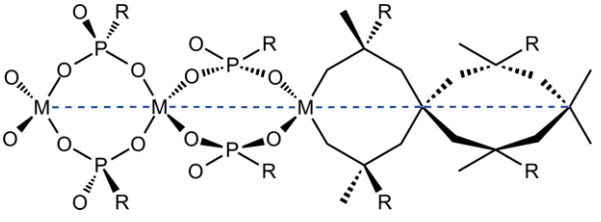

Figure 6. Eight-membered $M_2P_2O_4$ ring with defined angle for straightened chain.

The same structural motif is given in the compound Co-CAU-36 with a t-Co-8mpr forming a one-dimensional chain. Compared to the same linker with a discrete $Zn_2P_6O_{18}$ unit in the IPCE-1Ni, forming a t-Zn-8mpr as well, the surface area drops from 700 $m^2\ g^{-1}$ to 209 $m^2\ g^{-1}$. Therefore, it is believed that the formation of a one-dimensional chain gives access to a more ordered and bigger void volume (12.5 Å in diameter when unoccupied)[80] compared to a denser structure with a smaller void volume (6.5 Å).[81] To exclude the effect of the metal in both complexes the tetrahedral covalent radii of Co and Zn are given with 1.256 Å and 1.304 Å[89] and are very comparable in size.

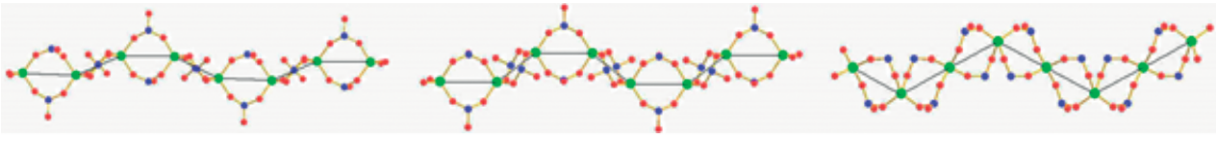

Figure 7. Left to right: Co-H_4-MTPPA, Zn_2-H_4-MTPPA, Zn_2-H_4-STPPA with defined intersections, green: Co or Zn, blue: P, red: O.

Minireview
doi.org/10.1002/ejic.201901291

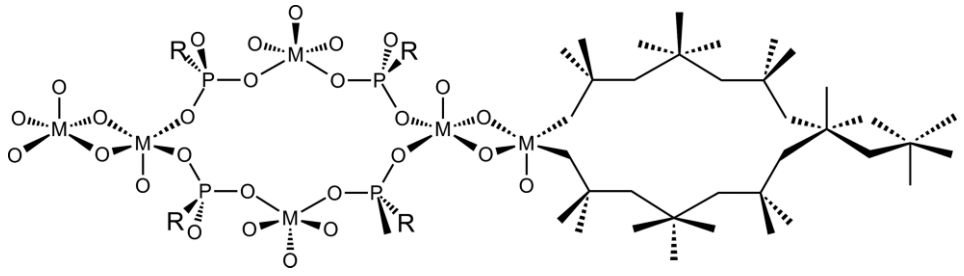

Figure 8. $M_4P_4O_8$ and M_2O_2 units.

Square Pyramidal or Trigonal Bipyramidal Metal Coordination

The common structure in the components $Pb_3(H_3L)_2(H_2O)$, CALF-33-Et_2H and CAU-14 is a square-pyramidal coordinated metal center and the formation of one-dimensional chains. The $Pb_3(H_3L)_2(H_2O)$ generates a one-dimensional chain with alternating sixteen-membered rings ($Pb_4P_4O_8$) and {Pb_2O_2} units (Figure 8).

In CALF-33-Et_2H there are two different chains involved (Figure 1). The copper atoms are either square planar or square-pyramidal coordinated. In case of the square-pyramidal coordinated copper a double chain with s.py.-Cu-8mpr is generated combining two one-dimensional chains via {Cu_2O_2} units (Figure 9 for reference).

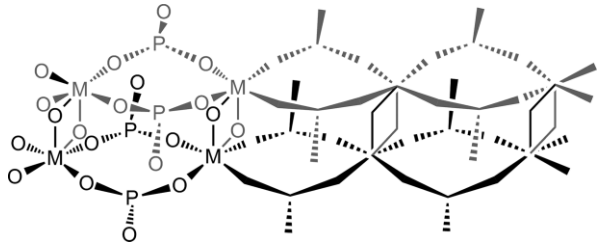

Figure 9. $M_2P_2O_4$ eight-membered rings connected by M_2O_2 units forming a double chain.

CAU-14 generates one-dimensional chains with trimeric $Cu_3O_9(H_2O)_3$ units with eight-membered $Cu_2P_2O_4$ rings and connects via the phosphonate linkers (Figure 10).

Due to the short linker $Pb_3(H_3L)_2(H_2O)$ composed of a quite dense structure with small slits of 4.4 Å × 8.2 Å and 3.5 Å × 8.2 Å. CAU-14 and CALF-33-Et_2H compose of similar linker sizes and generate pores with diameter of 9.4 Å and 7.2 Å × 16.1 Å. The BET surface areas are 647 $m^2\,g^{-1}$ and 810 $m^2\,g^{-1}$ respectively. The structural variety for pentagonal coordinated metal centers allows the formation of interesting structural motives due to the flexibility of the square pyramidal polyhedrons and the easy transformation to a trigonal bipyramidal polyhedrons. Up to date there are a limited number of compounds showing penta coordinated metal atoms in P-MOFs. But a high variety of structures is expected, and further publications are probably going to show a trend in metal-phosphonates.

Octahedral Metal Coordination

The structural motif of the following compounds UPG-1, Zr-CAU-30 and Zr-H_4-STPPA is an octahedral coordination around the Zr atom and the formation of o-Zr-8mpr in one-dimensional chains (Figure 11). This structure is also regarded with the tetragonal coordinated metal atoms. The difference is that a one-dimensional chain composed of tetrahedrons can exist in a bend form as described previously. Thanks to the four equatorial and two axial ligands that is not the case for octahedral coordinated metal atoms in one-dimensional chains. In most cases the equatorial ligands make up the connection in the chain and the axial coordination sites are filled with water molecules or connect to other linker molecules.

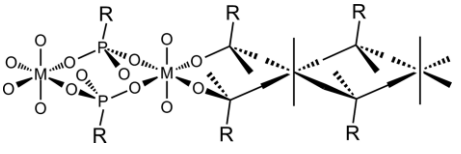

Figure 11. $M_2P_2O_4$ eight-membered ring for octahedral metal centers.

The compared Zrbtbp-a[90] consists of a layered structure of short chains containing three Zr octahedrons with o-Zr-8mpr (Figure 12). The extended inorganic connectivity is missing. Within the short chain the central Zr atom is coordinated by six bidentate phosphonate groups and the two terminal Zr atoms are connected by three monodentate phosphonate groups each. Due to the missing connectivity the layers are shifted

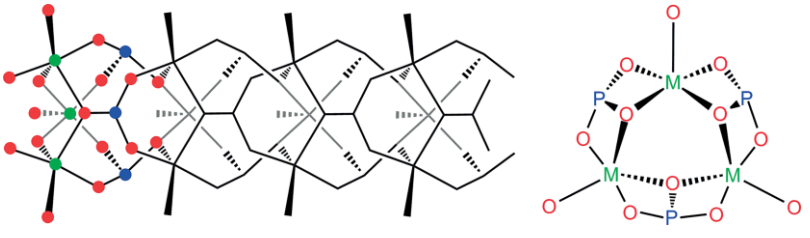

Figure 10. View along a-axis (left) and c-axis (right) of trimeric $Cu_3O_9(H_2O)_3$ chain.

Minireview
doi.org/10.1002/ejic.201901291

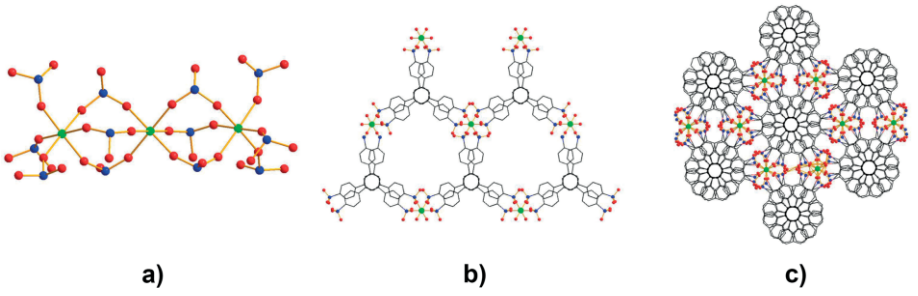

Figure 12. Zrbtbp-a (a) IBU chain of three Zr atoms, (b) one layer from view along c-axis, (c) multiple layer from view along c-axis with capped voids, green: Zr, blue: P, red: O.

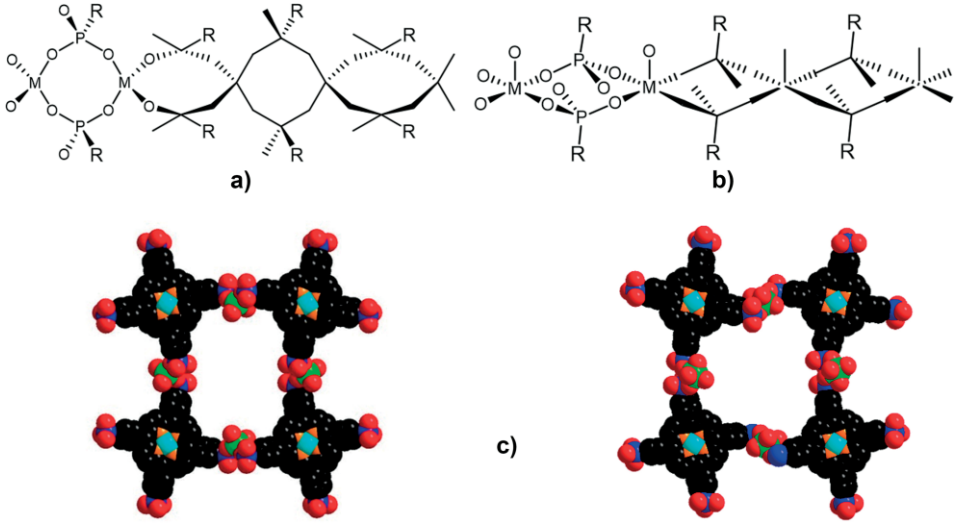

Figure 13. Comparison of one-dimensional chains of (a) tetragonal metal centers, (b) octahedral metal centers, and (c) space filling structures of Co-Cau-36 (left) and Zr-CAU-30 (right); black: C, blue: P, red: O, green: Co or Zr, orange: N, cyan: Ni.

and the voids are capped by adjacent layers. Therefore, the BET surface area was calculated to be as low as 10 $m^2 g^{-1}$. Compared to UPG-1 with a one-dimensional chain containing octahedral Zr atoms and void channels through the whole system, the BET surface area is considerably larger with 410 $m^2 g^{-1}$.

The difference between Zr-CAU-30 and Co-CAU-36 is the coordination of the metal atom. The M-8mpr, M = o-Zr or t-Co, differ in their constitution due to the different metal coordination. Therefore, the Zr-CAU-30 is more uniform and allows more organized and bigger voids then the compared Co-CAU-36. The crystallographic data shows rectangular voids for both components with different sizes. While Co-CAU-36 (Figure 13 left) got a void diameter of 12.5 Å the Zr-CAU-30 (Figure 13 right) got a slightly bigger voids with a diameter of 13 Å. This reflects the BET surfaces with 700 $m^2 g^{-1}$ compared to 970 $m^2 g^{-1}$. Therefore, the previously mentioned straightening of the chain produces more uniform and bigger voids allowing higher surface areas.

On the other hand tetrahedral linkers provide different mechanism on porosity compared to the planar porphyrin cored linkers. Octahedral coordination environment of Zr-H_4-STPPA allowed the coordination of more H_4-STPPA units around octahedral Zr leading more dense network while tetrahedral, Zn_2-H_4-STPPA opened up the distance between the linkers resulting in a higher BET surface area while Zr-H_4-STPPA is non-porous. Previous results[56] show that the known H_8-MTPPA linkers generate higher surface areas compared to the MOFs synthesized with H_8-STPPA linker.

Metal Clusters

There are still very limited number of phosphonate-MOFs that have metal clusters as IBUs. Two of such phosphonate-MOFs also have the monomeric 8-membered rings observed in the 1D chains as IBUs (See Figure 7). IBUs of Ni-CAU-29 (Figure 14a) and IPCE-1Ni (Figure 14b) are connected with the same linker Ni-H_8-TPPA but do not form any chain structures like Zr-CAU-30 and Co-CAU-36. In Ni-CAU-29 there are Ni-Ni distances of 3.19 Å and 5.12 Å. The smaller distances belong to the Ni_2O_2 cluster and therefore a formation of one-dimensional chains is not given to the bigger distances between the linkers. The same goes for IPCE-1Ni where the Ni-Ni distance between the linkers changes frequently between 6.22 Å and 4.98 Å. The distances between Zn-Zn in the distinct t-Zn-8mpr with 4.64 Å compared is smaller. A possible explanation appears by looking at the linker. The tetratopic porphyrin core with its π-conjugated system is planar with except for the phenyl rings (Figure 15). These can rotate along the central axis and extend to the required

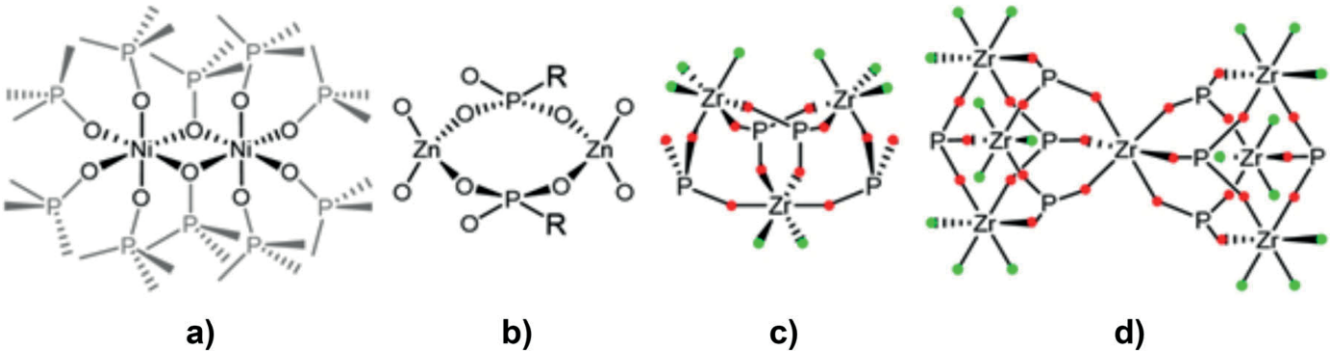

Figure 14. Structures of (a) Ni_2O_{10} cluster, (b) distinct $Zn_2P_2O_4$ ring, (c) $Zr_3P_4O_{10}F_8$ cluster, (d) $Zr_7P_8O_{22}F_{16}$ cluster; green: F, red: O.

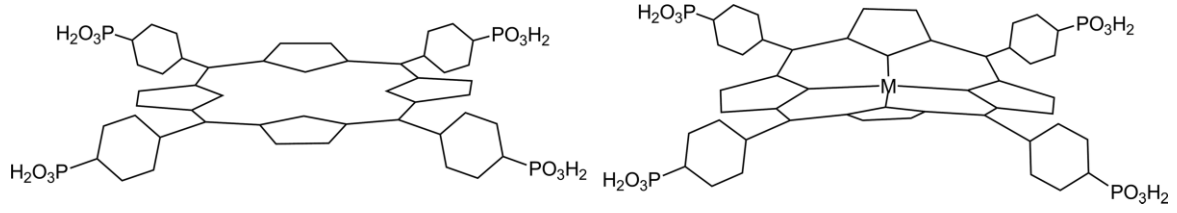

Figure 15. Schematic visualization of planar porphyrin core and saddle conformation. Double bonds omitted for clarity.[44]

space. Adding a suitable metal atom, the porphyrin core will bend into a saddle conformation and takes up more space, which is not provided by the metal-metal interactions.

In the other two structures, molecular IBUs have been synthesized via coordinated fluorine atoms in at least two positions around the octahedral coordination sphere of Zr to block the oligomeriation of the IBU into 1D chains. In comparison with other Zr-MOFs generated with a solvothermal or hydrothermal reaction the compounds SZ-2 and SZ-3 were generated by an ionothermal reaction providing different reaction dynamics. [59]

Conclusion

In conclusion, we have presented the known and persistent design patterns observed in the inorganic building units of phosphonate-MOFs. The most persistent structural motif observed in phosphonate-MOFs is the eight-membered M-O-P-O-M-O-P-O rings and the one dimensional IBUs comprising the corner shared such rings as monomers. We have further compared the different zero-dimensional inorganic building units and the resulting MOFs different linkers geometries. The rich conformational changes between tetrahedral and octahedral metal centers in M-O-P-O-M-O-P-O rings have generated flexible BET surface areas in phosphonate-MOFs. The observed conformational flexibility of one-dimensional IBUs of phosphonate MOFs, presence of tetrahedral metal centers facing the pore sites and square planar metals in porphyrin rings are clear indications for the small molecule storage or separation such as CO_2 and H_2S. Furthermore, we showed possible pathways to build up desired framework patterns using multi branched phosphonate linkers in Y-, X-, and X-tetrahedral geometries to reach well-defined pores. The current phosphonate MOFs has already generated variety of applications ranging from proton conductivity, catalysis, magnetism as well as biological and food chemistry applications. The identification of such persistent IBUs would pave new ways to isoreticular expansions of phosphonate MOFs and therefore creating a broader catalogue of synthetic approaches and applications.

In addition, we provided a new nomenclature for one-dimensional IBUs for phosphonate MOFs. The abbreviations used for the coordination of the metal atoms are: *t* = tetrahedral; s.pl. = square planar; s.py = square pyramidal; o = octahedral; 8mpr = 8-membered phosphonate ring(s).

Acknowledgments

Gündoğ Yücesan would like to thank the DFG for funding his work with grant number DFG YU 267/2-1 and Jens Beckmann would like to thank the DFG for funding his work with grant number BE 3716/9-1

Keywords: Metal-organic frameworks · Phosphonate ligands · Inorganic building units · Chain structures · Linker geometries

[1] Y. Liu, M. O'Keeffe, M. M. Treacy, O. M. Yaghi, *Chem. Soc. Rev.* **2018**, *47*, 4642–4664.
[2] H. Furukawa, K. E. Cordova, M. O'Keeffe, O. M. Yaghi, *Science* **2013**, *341*, 1230444.
[3] M. Ranocchiari, J. A. Van Bokhoven, *Phys. Chem. Chem. Phys.* **2011**, *13*, 6388–6396.
[4] P. Horcajada, T. Chalati, C. Serre, B. Gillet, C. Sebrie, T. Baati, J. F. Eubank, D. Heurtaux, P. Clayette, C. Kreuz, J. Chang, Y. K. Hwang, V. Marsaud, P. Bories, L. Cynober, S. Gil, G. Férey, P. Couvreur, R. Gref, *Nat. Mater.* **2010**, *9*, 172–178.
[5] P. Horcajada, R. Gref, T. Baati, P. K. Allan, G. Maurin, P. Couvreur, G. Férey, R. E. Morris, C. Serre, *Chem. Rev.* **2012**, *112*, 1232–1268.
[6] S. Rojas, T. Baati, L. Njim, L. Manchego, F. Neffati, N. Abdeljelil, S. Saguem, C. Serre, M. F. Najjar, A. Zakhama, P. Horcajada, *J. Am. Chem. Soc.* **2018**, *140*, 9581–9586.

[7] K. J. Hartlieb, D. P. Ferris, J. M. Holcroft, I. Kandela, C. L. Stern, M. S. Nassar, Y. Youssry, J. Botros, J. F. Stoddart, *Mol. Pharm.* **2017**, *14*, 1831–1839.
[8] K. J. Hartlieb, J. M. Holcroft, P. Z. Moghadam, N. A. Vermeulen, M. M. Algaradah, M. S. Nassar, Y. Y. Botros, R. Q. Snurr, J. F. Stoddart, *J. Am. Chem. Soc.* **2016**, *138*, 2292–2301.
[9] P. Siman, C. A. Trickett, H. Furukawa, O. M. Yaghi, *Chem. Commun.* **2015**, *51*, 17463–17466.
[10] B. Zhang, Y. Luo, K. Kanyuck, G. Bauchan, J. Mowery, P. Zavalij, *J. Agric. Food Chem.* **2016**, *64*, 5164–5170.
[11] L. Sun, M. G. Campbell, M. Dincă, *Angew. Chem. Int. Ed.* **2016**, *55*, 3566–3579; *Angew. Chem.* **2016**, *128*, 3628.
[12] L. Yang, X. He, M. Dincă, *J. Am. Chem. Soc.* **2019**, *141*, 10475–10480.
[13] L. S. Xie, L. Sun, R. Wan, S. S. Park, J. A. DeGayner, C. H. Hendon, M. Dincă, *J. Am. Chem. Soc.* **2018**, *140*, 7411–7414.
[14] E. M. Miner, S. S. Park, M. Dincă, *J. Am. Chem. Soc.* **2019**, *141*, 4422–4427.
[15] C. Yang, R. Dong, M. Wang, P. S. Petkov, Z. Zhang, M. Wang, P. Han, M. Ballabio, S. A. Bräuninger, Z. Liao, J. Zhang, F. Schwotzer, E. Zschech, H.-H. Klauss, E. Cánovas, S. Kaskel, M. Bonn, S. Zhou, T. Heine, X. Fen, *Nat. Commun.* **2019**, *10*, 3260.
[16] A. M. Wright, Z. Wu, G. Zhang, J. L. Mancuso, R. J. Comito, R. W. Day, C. H. Hendon, J. T. Miller, M. Dincă, *Chem* **2018**, *4*, 2894–2901.
[17] C. Jin, S. Zhang, Z. Zhang, Y. Chen, *Inorg. Chem.* **2018**, *57*, 2169–2174.
[18] G. M. Espallargas, E. Coronado, *Chem. Soc. Rev.* **2018**, *47*, 533–557.
[19] E. Coronado, G. M. Espallargas, *Chem. Soc. Rev.* **2013**, *42*, 1525–1539.
[20] C. T. P. da Silva, A. J. Howarth, M. Rimoldi, T. Islamoglu, A. W. Rinaldi, J. T. Hupp, *Isr. J. Chem.* **2018**, *58*, 1164–1170.
[21] T. Rhauderwiek, H. Zhao, P. Hirschle, M. Döblinger, B. Bueken, H. Reinsch, D. De Vos, S. Wuttke, U. Kolb, N. Stock, *Chem. Sci.* **2018**, *9*, 5467–5478.
[22] M. T. Wharmby, G. M. Pearce, J. P. S. Mowat, J. M. Griffin, S. E. Ashbrook, P. A. Wright, L.-H. Schilling, A. Lieb, N. Stock, S. Chavan, S. Bordiga, E. Garcia, G. D. Pirngruber, M. Vreeke, L. Gora, *Microporous Mesoporous Mater.* **2012**, *157*, 3–17.
[23] S. R. Miller, G. M. Pearce, P. A. Wright, F. Bonino, S. Chavan, S. Bordiga, I. Margiolaki, N. Guillou, G. Férey, S. Bourrelly, P. L. Llewellyn, *J. Am. Chem. Soc.* **2008**, *130*, 15967–15981.
[24] M. J. Beier, W. Kleist, M. T. Wharmby, R. Kissner, B. Kimmerle, P. A. Wright, J.-D. Grunwaldt, A. Baiker, *Chem. Eur. J.* **2012**, *18*, 887–898.
[25] R. S. Pillai, H. Jobic, M. M. Koza, F. Nouar, C. Serre, G. Maurin, N. A. Ramsahye, *ChemPhysChem* **2017**, *18*, 2739–2746.
[26] N. Hermer, M. T. Wharmby, N. Stock, *Z. Anorg. Allg. Chem.* **2017**, *643*, 137–140.
[27] Z. Kong, Z. Nui, L. He, Q. Chen, L. Zhou, Y. Cheng, Q. Guan, *New J. Chem.* **2018**, *42*, 16985–16991.
[28] V. Benoit, R. S. Pillai, A. Orsi, P. Normand, H. Jobic, F. Nouar, P. Billemont, E. Bloch, S. Bourrelly, T. Devic, P. A. Wright, G. de Weireld, C. Serre, G. Maurin, P. L. Llewellyn, *J. Mater. Chem. A* **2016**, *4*, 1383–1389.
[29] A. Schütrumpf, A. Duthie, E. Lork, G. Yücesan, J. Beckmann, *Z. Anorg. Allg. Chem.* **2018**, *644*, 1134–1142.
[30] H. Deng, S. Grunder, K. E. Cordova, C. Valente, H. Furukawa, M. Hmadeh, F. Gándara, A. C. Whalley, Z. Liu, S. Asahina, H. Kazumori, M. O'Keeffe, O. Terasaki, J. F. Stoddart, O. M. Yaghi, *Science* **2012**, *336*, 1018–1023.
[31] H.-C. Zhou, S. Kitagawa, *Chem. Soc. Rev.* **2014**, *43*, 5415–5418.
[32] M. S. Cohen, *J. Am. Chem. Soc.* **2017**, *139*, 2855–2863.
[33] M. Kim, J. F. Cahill, H. Fei, K. A. Prather, S. M. Cohen, *J. Am. Chem. Soc.* **2012**, *134*, 18082–18088.
[34] O. M. Yaghi, M. O'Keeffe, N. W. Ockwig, H. K. Chae, M. Eddaoudi, J. Kim, *Nature* **2003**, *423*, 705–714.
[35] A. Schoedel, M. Li, D. Li, M. O'Keeffe, O. M. Yaghi, *Chem. Rev.* **2016**, *116*, 12466–12535.
[36] G. Férey, *Eur. J. Inorg. Chem.* **2016**, 4275–4277.
[37] K. J. Gagnon, H. P. Perry, A. Clearfield, *Chem. Rev.* **2012**, *112*, 1034–1054.
[38] G. Yücesan, Y. Zorlu, M. Stricker, J. Beckmann, *Coord. Chem. Rev.* **2018**, *369*, 105–122.
[39] S. J. Shearan, N. Stock, F. Emmerling, J. Demel, P. A. Wright, K. D. Demadis, M. Vassaki, F. Costantino, R. Vivani, S. Sallard, I. Ruiz Salcedo, A. Cabeza, M. Taddei, *Crystals* **2019**, *9*, 270.
[40] S. Bao, G. K. H. Shimizu, L. Zheng, *Coord. Chem. Rev.* **2019**, *378*, 577–594.
[41] C. Gao, J. Ai, H. Tian, D. Wub, Z. Sun, *Chem. Commun.* **2017**, *53*, 1293–1296.
[42] A. Bulut, Y. Zorlu, R. Topkaya, B. Aktaş, S. Doğan, H. Kurt, G. Yücesan, *Dalton Trans.* **2015**, *44*, 12526–12529.
[43] Y. Zorlu, D. Erbahar, A. Çetinkaya, A. Bulut, T. S. Erkal, A. Ö. Yazaydın, J. Beckmann, G. Yücesan, *Chem. Commun.* **2019**, *55*, 3053–3056.
[44] M. Maares, M. M. Ayhan, K. B. Yu, A. O. Yazaydin, K. Harmandar, H. Haase, J. Beckmann, Y. Zorlu, G. Yücesan, *Chem. Eur. J.* **2019**, *25*, 11214–11217.
[45] M. Taddei, F. Costantino, R. Vivani, *Eur. J. Inorg. Chem.* **2016**, 4300–4309.
[46] J. K. Zaręba, *Inorg. Chem. Commun.* **2017**, *86*, 172–186.
[47] P. Bhanja, J. Na, T. Jing, J. Lin, T. Wakihara, A. Bhaumik, Y. Yamauchi, *Chem. Mater.* **2019**, *31*, 5343–5362.
[48] D. Sahoo, R. Suriyanarayanan, V. Chadrasekhar, *Dalton Trans.* **2014**, *43*, 10898–10909.
[49] R. A. Coxall, S. G. Harris, D. K. Henderson, S. Parsons, P. A. Tasker, R. E. P. Winpenny, *J. Chem. Soc., Dalton Trans.* **2000**, *14*, 2349–2356.
[50] G. Yücesan, V. Golub, C. J. O'Connor, J. Zubieta, *Solid State Sci.* **2005**, *7*, 133–139.
[51] A. Bulut, M. Maares, K. Atak, Y. Zorlu, B. Çoşut, J. Zubieta, J. Beckmann, H. Haase, G. Yücesan, *CrystEngComm* **2018**, *20*, 2152–2158.
[52] A. Clearfield, K. Demadis in *Metal Phosphonate Chemistry: From Synthesis to Applications*, Royal Society of Chemistry, Cambridge, **2011**.
[53] D. M. Poojary, B. Zhang, P. Bellinghausen, A. Clearfield, *Inorg. Chem.* **1996**, *35*, 4942–4949.
[54] W. Ouellette, M. H. Yu, C. J. O'Connor, J. Zubieta, *Inorg. Chem.* **2006**, *45*, 3224–3239.
[55] W. Ouellette, M. H. Yu, C. J. O'Connor, J. Zubieta, *Inorg. Chem.* **2006**, *45*, 7628–7641.
[56] A. Schütrumpf, A. Bulut, N. Hermer, Y. Zorlu, E. Kirpi, N. Stock, A. Ö. Yazaydın, G. Yücesan, J. Beckmann, *ChemistrySelect* **2017**, *2*, 3035–3038.
[57] A. Schütrumpf, E. Kirpi, A. Bulut, F. L. Morel, M. Ranocchiari, E. Lork, Y. Zorlu, S. Grabowsky, G. Yücesan, J. Beckmann, *Cryst. Growth Des.* **2015**, *15*, 4925–4931.
[58] A. Bulut, Y. Zorlu, E. Kirpi, A. Çetinkaya, M. Wörle, J. Beckmann, G. Yücesan, *Cryst. Growth Des.* **2015**, *15*, 5665–5669.
[59] T. Zheng, Z. Yang, D. Gui, Z. Liu, X. Wang, X. Dai, D. Sheng, *Nat. Commun.* **2017**, *8*, 15369.
[60] M. Taddei, S. J. I. Shearan, A. Donnadio, M. Casciola, R. Vivani, F. Costantino, *Dalton Trans.* **2020**, Advance Article, DOI: https://doi.org/10.1039/C9DT02463H.
[61] B. S. Gelfand, R. P. Huynh, R. K. Mah, G. K. Shimizu, *Angew. Chem. Int. Ed.* **2016**, *55*, 14614–14617; *Angew. Chem.* **2016**, *128*, 14834.
[62] S. S. Iremonger, J. Liang, R. Vaidhyanathan, I. Martens, G. K. Shimizu, T. D. Daff, T. K. Woo, *J. Am. Chem. Soc.* **2011**, *133*, 20048–20051.
[63] T. Rhauderwiek, K. Wolkersdorfer, S. Oien-Odegaard, K. P. Lillerud, M. Wark, N. Stock, *Chem. Commun.* **2018**, *54*, 389–392.
[64] B. Wang, T. Rhauderwiek, A. K. Inge, H. Xu, T. Yang, Z. Huang, N. Stock, X. Zou, *Chem. Eur. J.* **2018**, *24*, 17429–17433.
[65] See ref.[21]
[66] N. Hermer, N. Stock, *Dalton Trans.* **2015**, *44*, 3720–3723.
[67] R. K. Mah, B. S. Gelfand, J. M. Taylor, G. K. H. Shimizu, *Inorg. Chem. Front.* **2015**, *2*, 273–277.
[68] B. S. Gelfand, J.-B. Lin, G. K. H. Shimizu, *Inorg. Chem.* **2015**, *54*, 1185–1187.
[69] S. Pili, S. P. Argent, C. G. Morris, P. Rought, V. Garcìa-Sakai, I. P. Silverwood, T. L. Easun, M. Li, M. R. Warren, C. A. Murray, C. C. Tang, S. Yang, M. Schröder, *J. Am. Chem. Soc.* **2016**, *138*, 6352–6355.
[70] M. Taddei, F. Costantino, F. Marmottini, A. Comotti, P. Sozzani, R. Vivani, *Chem. Commun.* **2014**, *50*, 14831–14834.
[71] S.-F. Tang, X.-X. Lv, L.-J. Li, C. Wang, X.-B. Zhao, *Inorg. Chem. Commun.* **2014**, *39*, 51–55.
[72] J. M. Taylor, R. K. Mah, I. L. Moudrakovski, C. I. Ratcliffe, R. Vaidhyanathan, G. K. H. Shimizu, *J. Am. Chem. Soc.* **2010**, *132*, 14055–14057.
[73] A. M. Shultz, O. K. Farha, J. T. Hupp, S. B. T. Nguyen, *J. Am. Chem. Soc.* **2009**, *131*, 4204–4205.
[74] X.-L. Yang, M.-H. Xie, C. Zou, Y. He, B. Chen, M. O'Keeffe, C.-D. Wu, *J. Am. Chem. Soc.* **2012**, *134*, 10638–10645.
[75] K. Sengupta, S. Chatterjee, S. Samanta, S. Bandyopadhyay, A. Dey, *Inorg. Chem.* **2013**, *52*, 2000–2014.
[76] L. Meng, Q. Cheng, C. Kim, W.-Y. Gao, L. Wojtas, Y.-S. Chen, M. J. Zaworotka, X. P. Zhang, S. Ma, *Angew. Chem. Int. Ed.* **2012**, *51*, 10082–10085; *Angew. Chem.* **2012**, *124*, 10229.

[77] D. Feng, Z.-Y. Gu, J.-R. Li, H.-L. Jiang, Z. Wei, H.-C. Zhou, *Angew. Chem. Int. Ed.* **2012**, *51*, 10307–10310; *Angew. Chem.* **2012**, *124*, 10453.
[78] H.-L. Jiang, D. Feng, K. Wang, Z.-Y. Gu, Z. Wei, Y.-P. Chen, H.-C. Zhou, *J. Am. Chem. Soc.* **2013**, *135*, 13934–13938.
[79] M. Ding, X. Cai, H.-L. Jiang, *Chem. Sci.* **2019**, *10*, 10209–10230.
[80] See ref.[64]
[81] Y. Y. Enakieva, A. A. Sinelshchikova, M. S. Grigoriev, V. V. Chernyshev, K. A. Kovalenko, I. A. Stenina, A. B. Yaroslavtsev, Y. G. Gorbunova, A. Y. Tsivadze, *Chem. Eur. J.* **2019**, *25*, 10552–10556.
[82] M. Maares, C. Keil, S. Thomsen, D. Günzel, B. Wiesner, H. Haase, *J. Trace Elem. Med. Biol.* **2018**, *49*, 296–304.
[83] J. M. Taylor, R. Vaidhyanathan, S. S. Iremonger, G. K. H. Shimizu, *J. Am. Chem. Soc.* **2012**, *134*, 14338–14340.
[84] T. Morimoto, K. Miura, *Langmuir* **1985**, *1*, 658–622.
[85] P. Küsgens, M. Rose, I. Senkovska, H. Fröde, A. Henschel, S. Siegle, S. Kaskel, *Microporous Mesoporous Mater.* **2009**, *120*, 325–330.
[86] J. Y. Lee, D. H. Olson, L. Pan, T. J. Emge, J. Li, *Adv. Funct. Mater.* **2007**, *17*, 1255–1262.
[87] W. M. Hayne in *CRC Handbook of Chemistry and Physics 92nd ed.*, CRC Press, Boca Raton, **2011**.
[88] A. Bulut, M. Wörle, Y. Zorlu, E. Kirpi, H. Kurt, J. Zubieta, S. Grabowsky, J. Beckmann, G. Yücesan, *Acta Crystallogr., Sect. B* **2017**, *73*, 296–303.
[89] P. Pyykkö, *J. Phys. Chem. A* **2015**, *119*, 2326–2337.
[90] M. Taddei, F. Costantino, R. Vivani, S. Sabatini, S.-H. Lim, S. M. Cohen, *Chem. Commun.* **2014**, *50*, 5737–5740.

Received: December 2, 2019